

Determination of the modulation transfer function for a time-gated fluorescence imaging system

Sarah Gundy

National University of Ireland, Galway
National Centre for Biomedical Engineering Science
Galway, Republic of Ireland
E-mail: sarah.gundy@nuigalway.ie

Wil Van der Putten

University College Hospital Galway
Department of Medical Physics and Bioengineering
Galway, Republic of Ireland

Andy Shearer

National University of Ireland, Galway
Department of Information Technology
Galway, Republic of Ireland

Daniel Buckton*

National University of Ireland, Galway
Galway, Republic of Ireland

Alan G. Ryder

National University of Ireland, Galway
National Centre for Biomedical Engineering Science
Galway, Republic of Ireland

Abstract. The use of fluorescence for cancer detection is currently under investigation. Presently, steady-state fluorescence detection methods are in use, but have limitations due to poor contrast between the fluorescence of the tumor and background autofluorescence. Improved contrast can be obtained with time-resolved techniques because of the differing lifetimes between autofluorescence and exogenous photosensitizers that selectively accumulate within tumor tissue. An imaging system is constructed using a fast-gated (200-ps) charge-coupled device (CCD) camera and a pulsed 635-nm laser diode. To characterize the ability of the system to transfer object contrast to an image, the modulation transfer function (MTF) of the system is acquired by employing an extended knife-edge technique. A knife-edge target is assembled by drilling a rectangular well into a block of polymethyl methacrylate (PMMA). The imaging system records images of the photosensitizer, chloroaluminum phthalocyanine tetrasulfonate (AIPcTS), within the well. AIPcTS was chosen to test the system because of its strong absorption of 635-nm, high fluorescence yield, and relatively long fluorescence lifetime (~ 7.5 ns). The results show that the system is capable of resolving 10^{-4} M AIPcTS fluorescence as small as 1 mm. The findings of this study contribute to the development of a time-gated imaging system using fluorescence lifetimes.
© 2004 Society of Photo-Optical Instrumentation Engineers. [DOI: 10.1117/1.1803550]

Keywords: time-gated imaging; tumor detection; modulation transfer function; chloroaluminum phthalocyanine tetrasulfonate; photosensitizer; knife-edge test.

Paper 03106 received Aug. 11, 2003; revised manuscript received Jan. 23, 2004, and Feb. 16, 2004; accepted for publication Mar. 16, 2004.

1 Introduction

Photodynamic therapy (PDT) is a relatively new treatment modality that utilizes light and a photochemically active drug (photosensitizer) that preferentially accumulates within tumor tissues.^{1–3} Many of the photosensitizers used for PDT also exhibit high fluorescence yields that can be utilized for tumor detection.^{4–6} The use of fluorescence for cancer detection could have several advantages over alternatives such as conventional white-light endoscopy. For example, in the treatment of lung cancer, a more desirable prognosis is achieved when the lesion is discovered in the intraepithelial (preinvasive) stage.^{7,8} However, intraepithelial neoplastic lesions are difficult to localize by conventional white-light bronchoscopy (WLB).^{7,9,10} Fluorescence bronchoscopy, when used as an adjunct to WLB, has been proven to improve physicians' ability to detect lung cancer by 6.3 times compared with conventional WLB alone.⁷

Steady-state fluorescence imaging techniques are presently in use.^{11,12} Unfortunately, these methods have limitations due to poor contrast between the fluorescence of the tumor and background autofluorescence.^{13,14} To compensate for autofluorescence, current steady-state fluorescence imaging methods require parallel imaging at several excitation or emission

wavelengths, followed by image processing to subtract the autofluorescence contribution or to form emission wavelength ratios.¹⁵ Time-resolved fluorescence imaging techniques could eliminate the need for: 1. numerous excitation sources and/or filters, and 2. complex image processing to eliminate autofluorescence.

Previously, filters have been used to distinguish excitation scatter and autofluorescence from the fluorescence signal of a photosensitizer. As excitation wavelengths in the red are increasing in use, it is more difficult to use filters to discriminate from a fluorescence signal that is also red. Alternatively, a nanosecond-pulsed excitation source can be used, and then the photosensitizer fluorescence exhibited by the tumor can be detected only after both the excitation light and autofluorescence has decayed.¹⁶ By using this method, only the longer-lived emission signal of the photosensitizer will be detected. Also, there will be no need for complex image processing as is needed for fluorescence lifetime imaging (FLIM). (see Fig. 1).

Preinvasive bronchial cancers are usually very small, for example, a previous study showed that the median surface diameter of carcinoma *in situ* was 8 mm.⁹ Thus, it is important that an imaging device is able to detect fluorescent objects of the same magnitude or smaller. The modulation transfer function (MTF) is a parameter that characterizes the

Address all correspondence to Dr. Sarah Gundy, National University of Ireland, National Centre for Biomedical Engineering Science, Galway, Ireland.

*Current affiliation: Department of 3D/4D Image Processing, GE Medical Systems, Kretztechnik GmbH, Tiefenbach 15, 4871, Zipf, Austria.

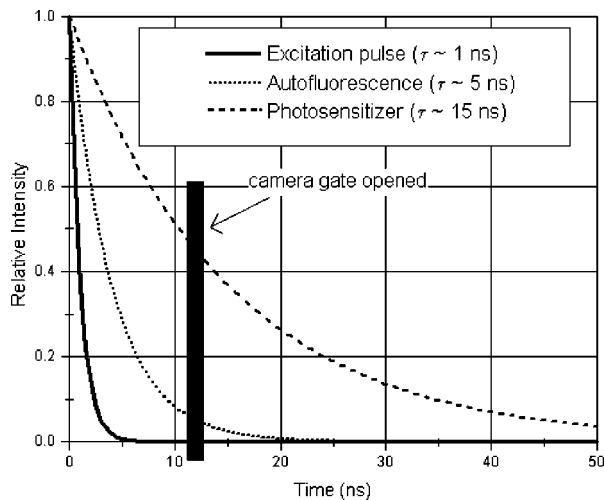


Fig. 1 Schematic depiction of the detection of a photosensitizer with a 15-ns fluorescence lifetime using a gated camera system.

resolution properties of a fluorescence imaging system. A simple method of determining the MTF of a digital image acquisition device is an extension of the traditional knife-edge technique.

The traditional knife-edge technique is a method used to calculate the MTF from an image of a knife edge, a target with a straight-edged, sharp discontinuity. Originally, the technique was created for characterizing acquisition devices that produce spatially continuous images such as conventional analog x-ray imaging systems that use film.¹⁷ The traditional approach relies on oversampling a continuous image with a scanning device. When the traditional knife-edge technique is applied to a digital imaging device, the image is not oversampled, which creates aliasing causing significant errors in calculating the MTF. An extension of the original technique, in which the knife edge is aligned slightly off perpendicular to the scan direction, generates a composite scan with a higher resolution than the sampling rate from which the MTF can be accurately obtained.¹⁸

Previous time-gated fluorescence imaging studies have used imaging systems with gate widths of 50 ns and repetition rates of 50 Hz.^{13,14,16,19–23} This investigation describes an improved fast-gated imaging system with shorter gating speeds (<1 ns) and higher repetition rates (100 kHz) than those used in prior investigations. Also, previous investigations of time-gated fluorescence imaging systems have not involved any quantitative analysis of spatial resolution. This investigation applies a spatial resolution measuring technique to perform a quantitative analysis of the developed imaging system. A novel knife-edge target designed specifically to test the time-gated fluorescence system was constructed to recover the edge response function, line spread function, and modulation transfer function.

2 Methods

2.1 Gated Imaging System

The time-gated imaging system is described by the set up shown in Fig. 2. The images were collected by an integrated, gateable intensified CCD camera system (4 Picos, Stanford

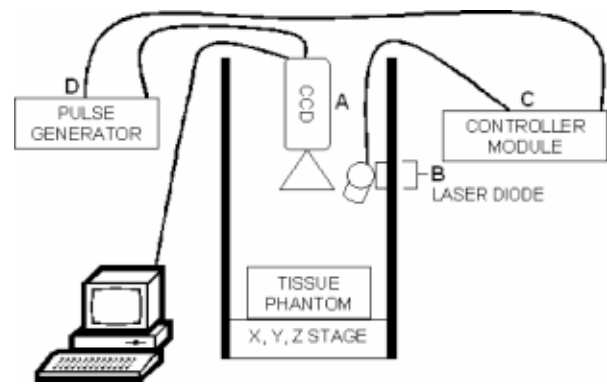


Fig. 2 Diagram of the time-gated imaging system.³⁰ (a) 4 Picos intensified camera, (b) 635-nm laser diode (NanoLED-02BN), (c) NanoLED controller module, and (d) Thurlby-Thander Pulse Generator TGP110.

Computer Optics, Munich, Germany). The camera has gating speeds as fast as 200 ps and a 25-mm dual-stage intensifier with an S25 enhanced photocathode. A Nikkor 50-mm f/1.4 lens was used to image an area of 9.0×9.0 cm. The excitation source was a 635-nm laser diode (NanoLED-02BN) powered by a NanoLED controller module (both from IBH, Glasgow, Scotland) and was positioned to illuminate the 9.0×9.0 cm imaging area as uniformly as possible. The laser diode produces a pulse width of <1 ns and a pulse energy of >100 pJ. The laser diode and camera were both pulsed by a Thurlby-Thander Pulse Generator TGP110 at a repetition rate of 100 kHz (1 pulse every 10 μs). All images were obtained using an MCP gain of 1400 V with an exposure time of 1 ns and an integration of 1000 frames. Image J software (National Institutes of Health, Bethesda, Maryland) was used to analyze all images.

2.2 System Gain

Unsigned 16-bit integers ranging from 0 to 65,535 are used to represent each pixel in an image. The count in a pixel is a direct measure of the number of electrons counted by the CCD frame. The variance method was used to determine the relationship of the count with the number of electrons and estimate the gain of the analog to digital converter (ADC).

The gain of the system G in terms of analog to digital units (ADU) per electron can be expressed by:

$$N_{\text{ADU}} = GxN_e, \quad (1)$$

where N_{ADU} is the average count and N_e is the average number of electrons generated due to photon detection. Hence, by plotting N_{ADU} on the y axis and the respective N_e on the x axis for varying light levels, the slope of the line will give G .

The standard deviation of the average count σ_{ADU} will also be subject to the gain of the system and therefore:

$$\sigma_{\text{ADU}} = Gx\sigma_e, \quad (2)$$

where σ_e is the standard deviation of the electron number. If both sides of Eq. (2) are squared, the result is:

$$\sigma_{\text{ADU}}^2 = G^2x\sigma_e^2. \quad (3)$$

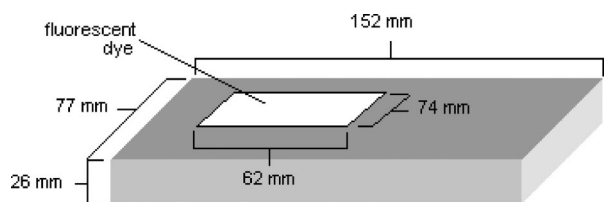


Fig. 3 Dimensions of the purpose-built fluorescence knife-edge target.

The standard deviation in a Poisson distribution is given by:²⁴

$$\sigma = \sqrt{N}. \quad (4)$$

Due to the Poisson distribution of the number of detected photons in a sampling interval, and hence the average number of generated electrons counted in the CCD frame, it can be assumed that:

$$N_e = \sigma_e^2. \quad (5)$$

Hence, dividing Eqs. (1) and (3) results in:

$$G = \frac{\sigma_{ADU}^2}{N_{ADU}}. \quad (6)$$

Therefore, it can be derived from Eqs. (1) and (6) that the average number of electrons that are counted by the CCD frame can be given by:

$$N_e = \frac{N_{ADU}^2}{\sigma_{ADU}^2}. \quad (7)$$

The average electron number was determined for a range of average counts. Images were collected with differing levels of light to vary the number of photons hitting the detector.

For accurate measurements, the dark count needed to be removed from the images. To remove the dark count, background images that were collected with no light being de-

tected were subtracted from all images used to determine the gain. A background image was obtained by averaging 10 images that were collected with the camera covered in black velvet with the lens cap on.

After the background image was subtracted to remove the dark count, the average count and standard deviation of the varying images were acquired. Histograms were collected from a consistent circular, 15 pixels in diameter region of interest (ROI) of each image to verify Poisson distribution. The average number of generated electrons was calculated from Eq. (7) using the data from the histograms. The average counts were plotted on the y axis and their corresponding calculated average electron numbers were plotted on the x axis. The slope of the line was calculated using MS Excel and determined as the gain. The gain was calculated to determine the relationship between the count in a pixel and the number of electrons counted by the CCD frame.

2.3 Determination of Modulation Transfer Function

A knife-edge target was designed specifically to test the developed time-gated fluorescence imaging system (see Fig. 3). A rectangular-shaped well (74 mm length × 62 mm width × 10 mm depth) was drilled into a block of polymethyl methacrylate (PMMA). All surfaces of the block except within the well were painted with nonfluorescent, matte black paint.

16-bit grayscale images were collected for 10⁻⁴ M chloroaluminum phthalocyanine tetrasulfonate (AlPcTS) and 0.2 M phosphate buffer (pH 7.2) placed within the target well. AlPcTS was chosen to test the system because of its strong absorption at 635-nm, high fluorescence yield (0.559),²⁵ and relatively long fluorescence lifetime (~7.5 ns)²⁶ compared to the other second generation photosensitizers (such as hypericin, methylene blue, n-aspartyl chlorin e6, and texaphyrins) that were considered.²⁷ Images were collected at delay times varying from 1.5 to 10.0 ns (in 0.5-ns increments) after the peak of the excitation pulse.

To obtain the modulation transfer function (MTF) of the imaging system, an extension of the knife-edge test was employed.¹⁸ The target was positioned at a slight angle (18

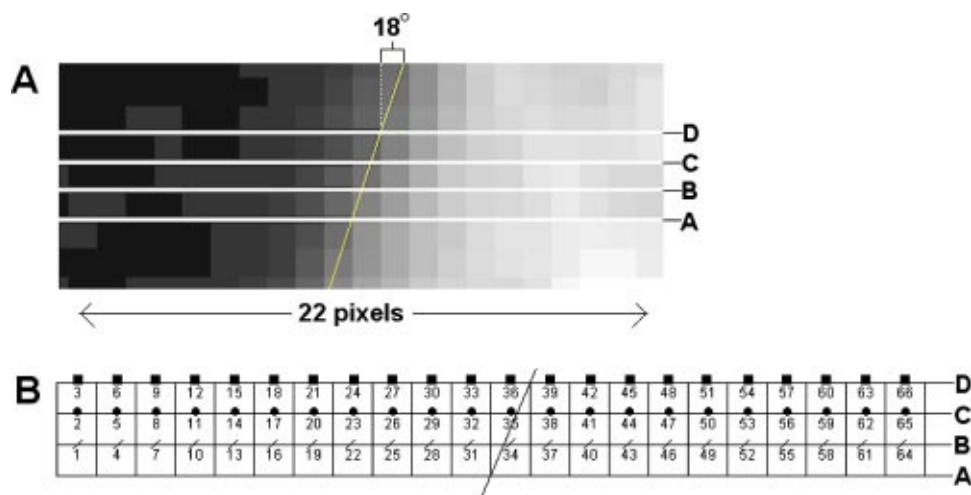


Fig. 4 (a) Image of pixels with knife edge skewed perpendicular and emphasized for illustrative purposes, and (b) schematic diagram of pixels with their assigned numbers representing their position in the composite edge response function. Locations A, B, and C correspond to three different alignments of the edge relative to the sampling coordinate. Positions A and D represent the two half-pixel shifted alignments.

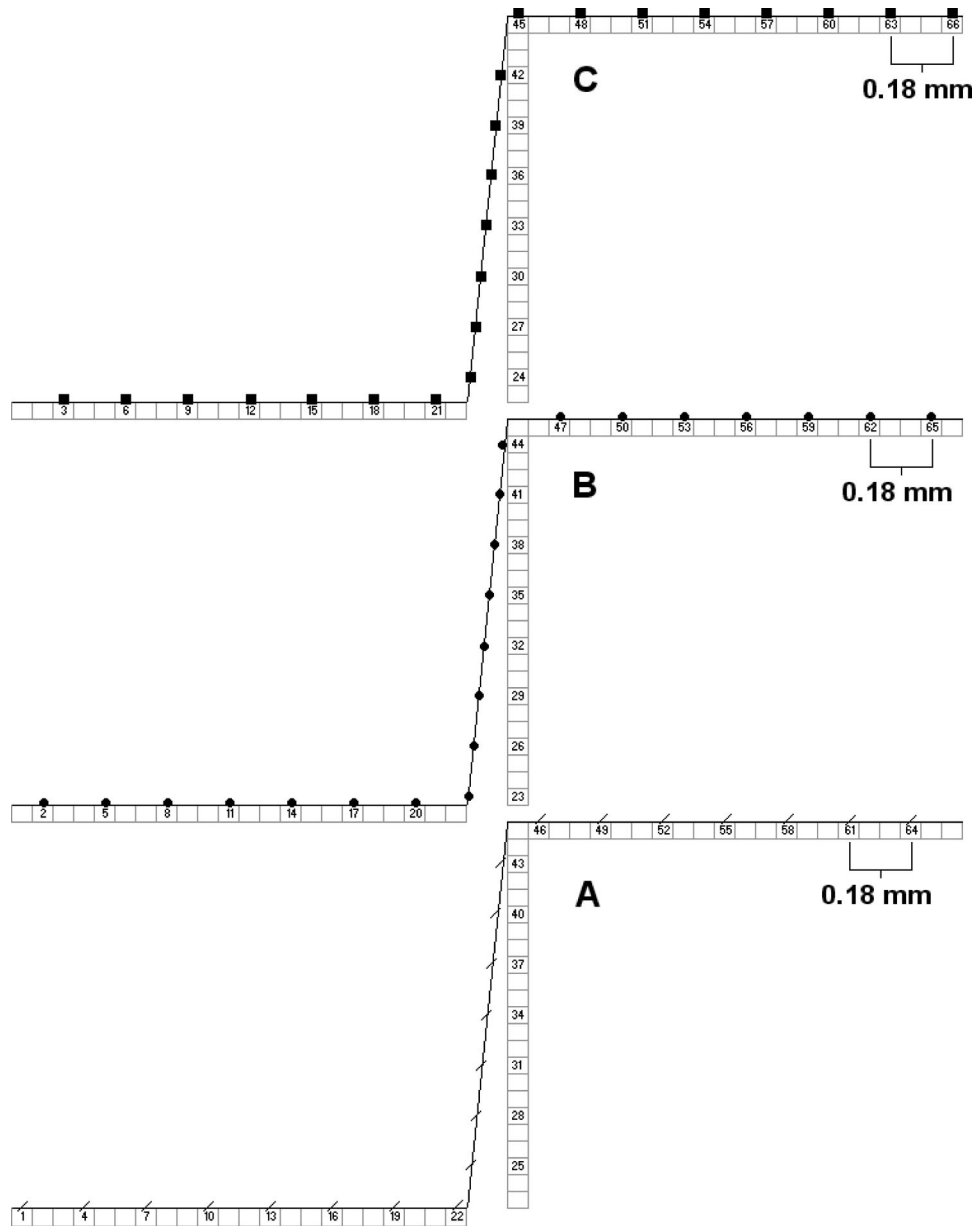


Fig. 5 Schematic diagram of the pixels and their assigned numbers used to obtain edge response functions with a sampling distance of 0.18 mm for locations A, B, and C.

deg) to the direction perpendicular to the scanning direction in deriving the edge response function (ERF), as shown in Fig. 4(a). Because of the slight angulation of the edge, three ERFs at locations A, B, and C depicted in Fig. 4(a), which correspond to three different alignments of the edge relative to the sampling coordinate, can be obtained in the range between the two different half-pixel shifted alignments [positions A and D in Fig. 4(a)].

Three ERFs were produced by obtaining pixel values across the image of the knife edge at locations A, B, and C as specified in Fig. 4(a). Each pixel value for the individual ERFs at locations A, B, and C were assigned a number representing their position in the composite ERF, as shown in Fig. 4(b). The individual ERFs for positions A, B, and C consist of 22 discrete data points with the same sampling

distance of 0.18 mm as demonstrated in Fig. 5. Thus, a total of 66 combined data points acquired from the three ERFs from A, B, and C can be employed to generate the composite ERF with a smaller sampling distance of 0.06 mm (see Fig. 6). Since the effective sampling distance becomes smaller, the effects of aliasing on the measured MTF can be eliminated.²⁸

Composite ERFs were obtained from images (with the dark count removed) for each delay time and then smoothed with sigmoidal fits generated by CurveExpert 1.3 (Daniel G. Hyams, Hixson, Tennessee). The linespread function (LSF) was then found by the numerical differentiation of each smoothed composite ERF. A Fourier transform of each determined LSF was performed by Microcal Origin 4.0 (OriginLab Corporation, Northampton, Massachusetts) to obtain the MTF for each delay time. Images were also collected with a line

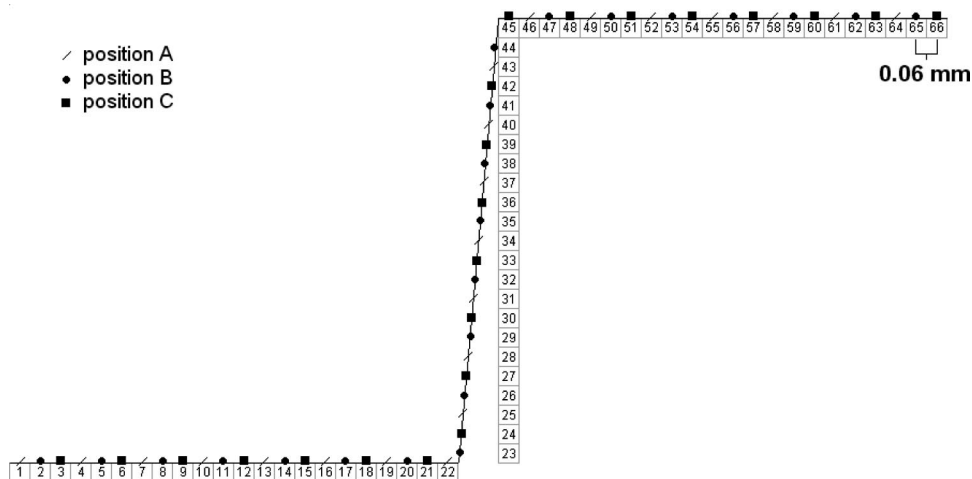


Fig. 6 Schematic diagram of the pixels and their assigned numbers used to obtain the composite edge response function with a sampling distance of 0.06 mm.

resolution test target placed on top of the well containing the 10^{-4} M AIPcTS following the same imaging procedures to obtain a subjective perception of the MTF.

3 Results and Discussion

Figure 7 shows the average count plotted against the average number of calculated electrons. The gain of the ADC for a MCP gain of 1400 V was found to be 107 ADU/e⁻. The figure shows that the imaging system exhibits good system linearity for counts ranging from 0 to 50,000.

The ERFs, LSFs, and MTFs at delay times between 4.5 and 6.0 ns are of particular interest because it is predicted that: 1. the fluorescence from the AIPcTS within the well will not have entirely decayed, and 2. the viewing of the AIPcTS will not be hindered from excitation scatter or autofluorescence. Figures 8(a) and 8(b) reveal smoothed ERFs for delay times of 4.5 to 6.0 ns [Fig. 8(a)], and 6.5 to 8.0 ns [Fig. 8(b)] in 0.5-ns increments. The figures demonstrate that as the delay

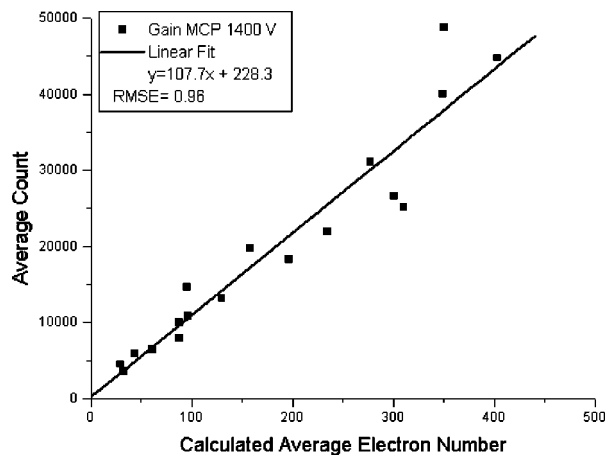


Fig. 7 Average count (ranging from 0 to 50,000) versus calculated average electron number (ranging from 0 to 500) for a MCP gain of 1400 V.

time increases, the slope and intensity of the ERFs decrease. This decrease is expected and corresponds to the decay of the AIPcTS fluorescence.

Figures 9(a) and 9(b) depict the LSFs for delay times of 4.5 to 6.0 ns [Fig. 9(a)] and 6.5 to 8.0 ns [Fig. 9(b)] in 0.5-ns increments. The figures show that as the delay time increases, the intensity decreases and the LSFs widen. The LSFs are somewhat skewed, which might be suggesting crosstalk or a slight misalignment of the target edge.

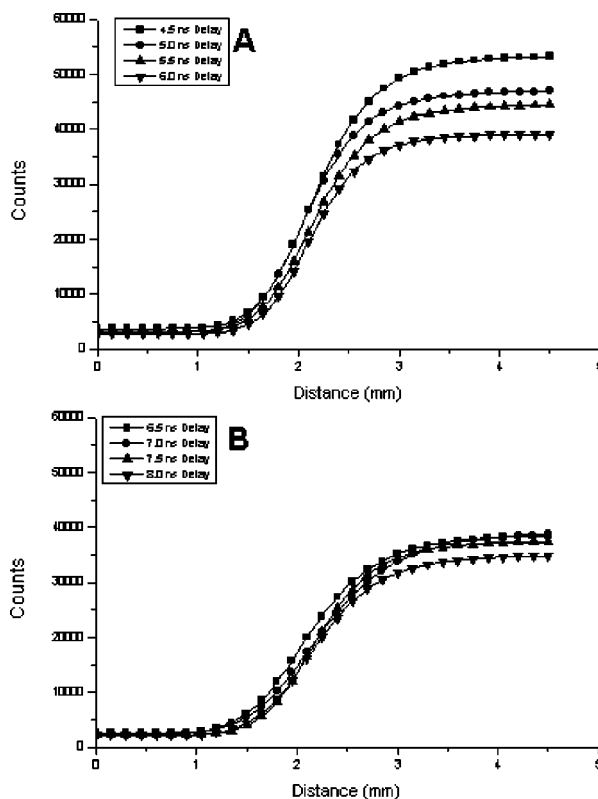


Fig. 8 Edge response functions for delay times of (a) 4.5 to 6.0 ns, and (b) 6.5 to 8.0 ns, in 0.5-ns increments.

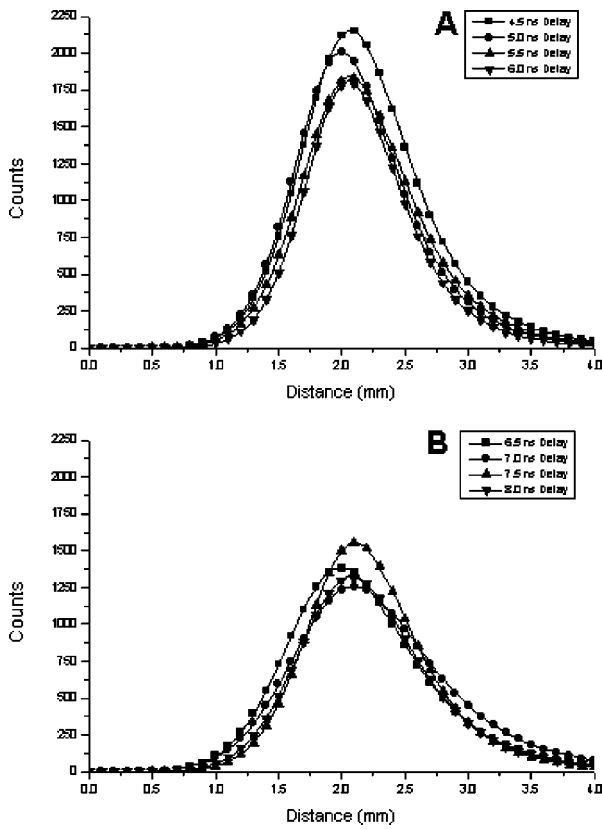


Fig. 9 Line spread functions for delay times of (a) 4.5 to 6.0 ns, and (b) 6.5 to 8.0 ns, in 0.5-ns increments.

Figures 10(a) and 10(b) show the MTFs for delay times of 4.5 to 6.0 ns, and 6.5 to 8.0 ns, respectively, in 0.5-ns increments. Since the MTF can realistically only be found within 10%,²⁹ error bars representing the standard deviations were added to the graphs, which indicate that the MTFs were indeed found within 10%. According to Figs. 10(a) and 10(b) the MTFs indicate that the developed imaging system should be capable of resolving 1 line pair/mm (lp/mm), or fluorescent objects as small as 1 mm for the specified delay times. The calculated resolution in this study is in agreement with a

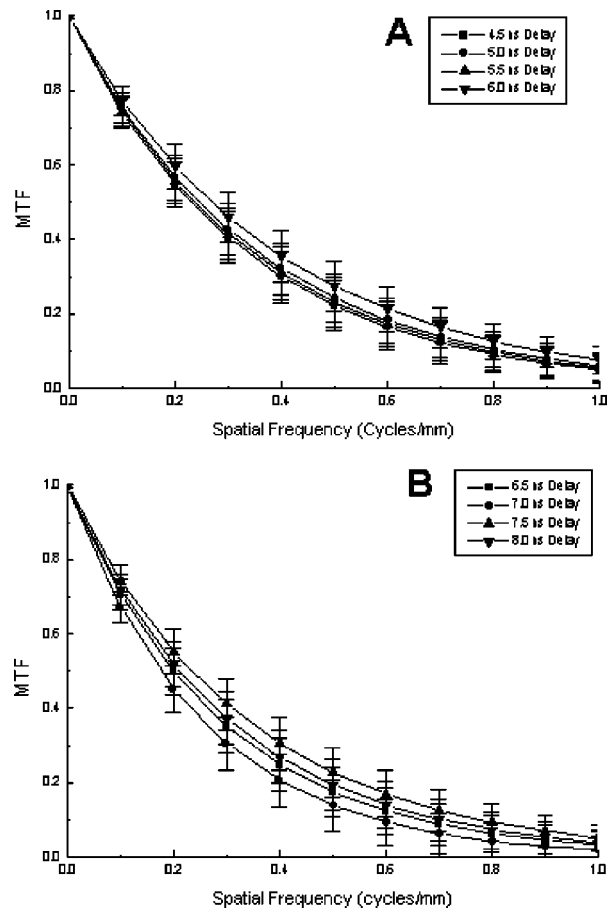


Fig. 10 Modulation transfer functions for delay times of (a) 4.5 to 6.0 ns, and (b) 6.5 to 8.0 ns, in 0.5-ns increments.

previous investigation, which demonstrates the constructed imaging system's ability to resolve 10^{-4} M AIPcTS fluorescence of 1 mm in diameter at depths ranging from 1 to 3 mm.³⁰

Figure 11 shows a line resolution test target placed on top of the 10^{-4} M AIPcTS at a 6.0-ns delay as an additional way to estimate the MTF. It can be seen that at 1 lp/mm the lines

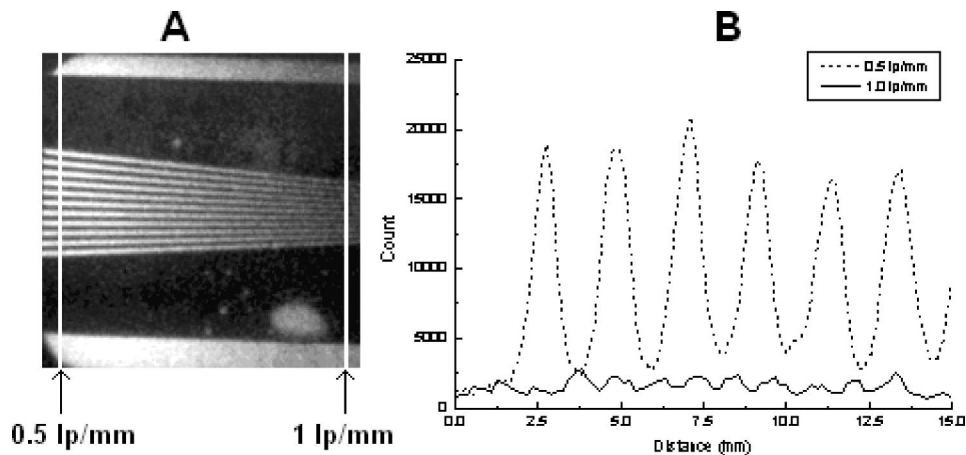


Fig. 11 (a) Line resolution test target placed on top of 10^{-4} M AIPcTS at a 6.0-ns delay, and (b) plot profiles for 0.5 and 1 lp/mm.

of the test target can be made out, which is in agreement with the quantitative results of the MTFs. Plot profiles are also given for both 0.5 and 1 lp/mm. Peaks and troughs can be clearly seen for the 0.5-lp/mm plot profile. The plot profile for 1 lp/mm is noisier, but peaks and troughs can still be made out, which also concurs with the resulting MTFs. Although the test target image does not determine a quantitative value for the MTF, it does show that the subjective perception of the image is in agreement with the MTFs calculated from the extended knife-edge technique.

4 Conclusions

In this study, a time-gated imaging system is developed to remove background excitation scatter and autofluorescence from distorting the fluorescence signal from a longer-lived photosensitizer within a tumor without the need for filters. An initial analysis of the imaging system is executed to determine the system's ability to resolve fluorescent objects.

The gain of the ADC is examined to establish the relationship between the count in a pixel and the number of electrons counted by the CCD frame. The system is shown to have a gain of ~ 107 ADU/e⁻ using an MCP gain of 1400 V and be linear within the operating conditions. The method used to estimate the gain in this study is simple, yet adequate enough to prove the linearity of the system. A more precise evaluation of the gain, such as varying the irradiance on the photocathode and measuring the output signal, is not required for this investigation and is the subject of further study.

The ESF, LSF, and MTF are determined for each delay time to determine the resolvability of the system. The calculated MTFs describe the contrast produced by the imaging system as a function of the spatial frequency of a fluorescent object. The MTFs show that a 10^{-4} M AIPcTS fluorescent object as small as 1 mm can be resolved by the system. In agreement to this, an image of a resolution test target shows that 1 lp/mm could be viewed. As far as the authors are aware, there have been no spatial resolution studies performed on other time-gated fluorescence imaging systems. Therefore, it is not possible to compare the current results to those of other systems.

It must be noted that the estimated resolution is for a simplified system using a macrolens. If the imaging system was connected with an endoscope, the resolution would need to be re-examined. This investigation shows that the extended knife-edge technique is adequate in estimating the spatial resolution of a time-gated fluorescence imaging system, and could easily be reapplied to evaluate the MTF of the system connected to an endoscope.

There are three things that deter the resolution in fluorescence imaging systems: 1. scattering of excitation light, 2. obscuring of the target due to autofluorescence, and 3. scattering of fluorescent light. The developed imaging system is adequate for limiting 1 and 2, which is a major improvement over existing systems. To remove 3, a camera with a gate width of a few picoseconds would be required, which does not currently exist. Therefore, degradation in resolution due to the scattering of fluorescence light could not be eliminated with the present system.

The findings of this study contribute to the development of a time-gated imaging system using fluorescence lifetimes. In

this investigation, a fast-gated imaging system with quicker gating speeds (1 ns) and repetition rates (100 kHz) than those used in prior investigations is designed. Because of its high resolvability and quick image acquisition, the development of the time-gated imaging system could make early cancer screening programs more feasible. Future investigations should be performed because of the system's proven potential.

Acknowledgments

This work was supported by the National Center for Biomedical Engineering Science as part of the Irish Higher Education Authority Program for Research in Third Level Institutions.

References

1. J. Fuchs and J. Thiele, "The role of oxygen in cutaneous photodynamic therapy," *Free Radic Biol. Med.* **24**(5), 835–847 (1998).
2. T. J. Dougherty, C. J. Gomer, B. W. Henderson, G. Jori, D. Kessel, M. Korbelik, J. Moan, and Q. Peng, "Photodynamic therapy," *J. Natl. Cancer Institute* **90**(12), 889–900 (1998).
3. M. Ochsner, "Photophysical and photobiological processes in the photodynamic therapy of tumours," *J. Photochem. Photobiol., B* **39**(1), 1–18 (1997).
4. M. Zandomenighi, C. Festa, C. A. Angeletti, G. Menconi, T. Sicuro, and I. Cozzani, "Detection of near-infrared porphyrin fluorescence excited in experimental animal tumours by the HeNe laser," *Lasers Med. Sci.* **3**, 99–102 (1988).
5. K. Furukawa, T. Okunaka, T. Tsuchida, N. Ikeda, T. Hiyoshi, Y. Yamamoto, H. Kumasaka, H. Sakai, C. Konaka, and H. Kato, "Laser-induced fluorescence endoscopy in the early detection of lung cancer using the photosensitizer," *Lung Cancer* **18**, 93 (1997).
6. V. I. Chissov, V. V. Sokolov, E. V. Filonenko, V. D. Menenkov, N. N. Zharkova, D. N. Kozlov, Yu. N. Polivanov, A. M. Prokhorov, R. L. Pykhov, and V. V. Smirnov, "Clinical fluorescence diagnostics in photodynamic carcinoma treatment with the photosensitizer Photogem," *Int. J. Gynaecol. Obstet.* **55**, 90 (1996).
7. S. Lam, T. Kennedy, M. Unger, Y. E. Miller, D. Gelmont, V. Rusch, B. Gipe, D. Howard, J. C. LeRiche, A. Coldman, and A. F. Gazdar, "Localization of bronchial intraepithelial neoplastic lesions by fluorescence bronchoscopy," *Chest* **113**(3), 696–702 (1998).
8. S. J. Winawer, A. G. Zauber, M. N. Ho, M. J. O'Brien, L. S. Gottlieb, S. S. Sternberg, J. D. Wayne, M. Schapiro, J. H. Bond, J. F. Panish, F. Ackroyd, M. Shike, R. C. Kurtz, L. Hornsby Lewis, H. Gerdes, and E. Stewart, "Prevention of colorectal cancer by colonoscopic polypectomy," *N. Engl. J. Med.* **329**(27), 1977–1981 (1993).
9. L. B. Woolner, "Pathology of cancer detected cytologically," in *Atlas of Early Lung Cancer*, pp. 107–213, National Cancer Institute, National Institute of Health, U.S. Department of Health and Human Services, Igaku-Shoin, New York (1983).
10. S. Lam, C. MacAulay, J. C. LeRiche, and B. Palcic, "Detection and localization of early lung cancer by fluorescence bronchoscopy," *Cancer* **89**(11), 2468–2473 (2000).
11. S. Lam, J. C. LeRiche, and C. MacAulay, "Laser-assisted bronchoscopy in the early detection and treatment of lung cancer," *Lung Cancer* **18**, 42 (1997).
12. M. Dal Fante, F. De Paoli, S. Pilotti, and P. Spinelli, "Fluorescence bronchoscopy in early detection of lung cancer," *Eur. J. Cancer* **32**, S8 (1996).
13. R. Cubeddu, G. Canti, A. Pifferi, P. Taroni, and G. Valentini, "Fluorescence lifetime imaging of experimental tumors in hematoporphyrin derivative-sensitized mice," *Photochem. Photobiol.* **66**(2), 229–236 (1997).
14. R. Cubeddu, G. Canti, P. Taroni, and G. Valentini, "Tumour visualization in a murine model by time-delayed fluorescence of sulpho-nated aluminium phthalocyanine," *Lasers Med. Sci.* **12**(3), 200–208 (1997).
15. C. Klinteberg, "On the use of light for the characterization and treatment of malignant tumours," Doctoral Thesis, Lund Institute of Technology (1999).
16. R. Cubeddu, P. Taroni, and G. Valentini, "Time-gated imaging system for tumour diagnosis," *Opt. Eng.* **32**(2), 320–325 (1993).
17. R. V. Shack, "Characteristics of an image-forming system," *J. Res. Natl. Bur. Stand.* **56**(5), 245–260 (1956).

18. S. E. Reichenbach, S. K. Park, and R. Narayanswamy, "Characterising digital image acquisition devices," *Opt. Eng.* **30**(2), 170–177 (1991).
19. R. Cubeddu, R. Ramponi, P. Taroni, G. Canti, L. Ricci, and R. Supino, "Time-gated fluorescence spectroscopy of porphyrin derivatives incorporated into cells," *J. Photochem. Photobiol., B* **6**(1–2), 39–48 (1990).
20. R. Cubeddu, G. Canti, P. Taroni, and G. Valentini, " δ -aminolevulinic acid induced fluorescence in tumour-bearing mice," *J. Photochem. Photobiol., B* **30**(1), 23–27 (1995).
21. R. Cubeddu, G. Canti, P. Taroni, and G. Valentini, "Study of porphyrin fluorescence in tissue samples of tumor-bearing mice," *J. Photochem. Photobiol., B* **29**(2–3), 171–178 (1995).
22. R. Cubeddu, G. Canti, P. Taroni, and G. Valentini, "Time-gated fluorescence imaging for the diagnosis of tumors in a murine model," *Photochem. Photobiol.* **57**(3), 480–485 (1993).
23. R. Cubeddu, P. Taroni, G. Valentini, and G. Canti, "Use of time-gated fluorescence imaging for diagnosis in biomedicine," *J. Photochem. Photobiol., B* **12**(1), 109–113 (1992).
24. G. Reike, *Detection of Light; From Ultraviolet to the Submillimeter*, Cambridge University Press, New York (2003).
25. J. W. Owens, R. Smith, R. Robinson, and M. Robins, "Photophysical properties of porphyrins, phthalocyanines, and benzochlorins," *Inorg. Chim. Acta* **279**(2), 226–231 (1998).
26. S. Gundy, W. van der Putten, A. Shearer, D. Buckton, A. G. Ryder, and M. Ball, "Time-gated fluorescence imaging of tetrasulfonated phthalocyanine dyes in a tissue phantom," *Proc. SPIE* **4876**, 109–119 (2003).
27. S. Gundy, W. van der Putten, A. Shearer, D. Buckton, A. G. Ryder, and M. Ball, "Time-resolved fluorescence studies of porphycene and tetrasulfonated dyes in varying solvents," *Proc. SPIE* **4432**, 299–309 (2001).
28. H. Fujita, D. Y. Tsai, T. Itoh, K. Doi, J. Morishita, K. Ueda, and A. Ohtsuka, "A simple method for determining the modulation transfer function in digital radiography," *IEEE Trans. Med. Imaging* **11**, 34–39 (1992).
29. G. D. Boremann, "MTF in Optical and Electro-Optical Systems," Short Course, Photonics West 2003, San Jose, CA 30 Jan. 2003.
30. S. Gundy, W. van der Putten, A. Shearer, D. Buckton, A. G. Ryder, and M. Ball, "The use of chloroaluminum phthalocyanine tetrasulfonate (AlPcTS) for time-delayed fluorescence imaging," *Phys. Med. Biol.* **49**(3), 359–369 (2004).